energies

MDPI

Article

Effects of Ramp Rate Limit on Sizing of Energy Storage Systems for PV, Wind and PV–Wind Power Plants

Micke Talvi *, Tomi Roinila and Kari Lappalainen

Electrical Engineering Unit, Tampere University, Korkeakoulunkatu 3, 33720 Tampere, Finland; tomi.roinila@tuni.fi (T.R.); kari.lappalainen@tuni.fi (K.L.)

* Correspondence: micke.talvi@tuni.fi

Abstract: As the share of highly variable photovoltaic (PV) and wind power production increases, there is a growing need to smooth their fast power fluctuations. Some countries have set power ramp rate (RR) limits that the output powers of power plants may not exceed. In this study, the effects of RR limit on the sizing of energy storage systems (ESS) for PV, wind, and PV–wind power plants are examined. These effects have been studied prior for PV power plants. However, for the wind and PV–wind power plants, the effects of the RR limit are studied comprehensively for the first time. In addition, the effects of the size of the power plant are considered. The study is based on climatic measurements carried out with a sampling frequency of 10 Hz for a period of 153 days. The modeling of the PV and wind powers and the simulation of the RR-based control algorithm of the ESS were completed using MATLAB. The results show that as the applied RR limit increased from 1%/min to 20%/min, the required relative energy capacities of the ESSs of the PV, wind, and PV–wind power plants decreased roughly 88%, 89%, and 89%, respectively. The required relative power capacities of the ESSs of the PV, wind, and PV–wind power plants decreased roughly 15%, 12%, and 20%, respectively. The utilization of the ESSs was found to decrease as the applied RR limit increased and as the size of the power plant grew.

Keywords: photovoltaic power; wind power; power ramp rate; power fluctuations; energy storage; power smoothing; energy storage sizing

Citation: Talvi, M.; Roinila, T.; Lappalainen, K. Effects of Ramp Rate Limit on Sizing of Energy Storage Systems for PV, Wind and PV–Wind Power Plants. *Energies* **2023**, *16*, 4313. https://doi.org/10.3390/en16114313

Academic Editors: Seppo Sierla, Mahdi Pourakbari-Kasmaei and Matti Vilkko

Received: 28 April 2023
Revised: 17 May 2023
Accepted: 23 May 2023
Published: 24 May 2023

1. Introduction

The share of electricity produced by photovoltaic (PV) and wind power plants will increase significantly in the future [1,2]. It is estimated that the share of renewable electricity generation is going to reach around 69% in the European Union by 2030 [1]. As the penetration levels of PV and wind power increase in the electric grid, the stability of the electric grid may suffer from the lack of inertia of these power generation sources. The fast power fluctuations of these power generation types are also likely cause issues in the electric grid [3]. Due to the unpredictable and intermittent nature of solar irradiance and wind, the output powers of PV power plants and wind power (WP) plants can fluctuate drastically. In [4], it was found that a maximum measured change in power was 43.8% of the rated power during one second for a small PV power plant. For a large PV power plant, power fluctuations as high as 70%/min of the rated power were observed using a 60 s time window [5]. For WP plants, the power fluctuations are slightly less drastic. In [6], it was found that the maximum measured power ramp rate (RR) was 7.3% of the rated power during a one-second time window for a 103.5 MW WP plant.

To prevent the issues caused by highly fluctuating power, some countries have set power RR limits that power plants need to comply with. For example, Puerto Rico has set an RR limit of 10%/min of the rated power of a power plant [7]. The power RR limit means the maximum power difference between the end points of a time interval [3]. In other words, the RR limit defines the maximum power RR that a power plant may feed into the grid.

A common solution to mitigate the power fluctuations of a power plant and to comply with the RR limits is to equip the power plant with an energy storage system (ESS). It is expected that the global installed capacity of utility-scale batteries is going to increase from roughly 10 GW/20 GWh to 60 GW/160 GWh between 2020 and 2026 [1]. The European Commission has similar estimations [2], and it expects that the need for flexibility in the electricity system is going to increase significantly. As ESSs are going to be installed globally in different power grids, the grid restrictions and RR limits are very likely to differ by country. The effects of different RR limits applied to the sizing of ESSs are therefore reasonable to investigate.

There are different control strategies to operate an ESS. One control strategy is an RR-based control algorithm. An RR-based control algorithm was used with a PV power plant in [8–12]. In these studies, the ESS of the PV power plant was sized for different RR limits. The basic idea behind RR-based control algorithms is that the ESS only operates when the power fluctuations of the power plant exceed the RR limit. In addition to the straightforward power fluctuation mitigation, some of the RR-based control algorithms are also programmed to control the energy level of the ESS. For example, in [8] an RR-based control algorithm ensured that the ESS had enough energy for a sudden shutdown at every moment, and in [9,10] the algorithm also controlled the state of charge of the ESS.

The power fluctuations of a WP plant can also be mitigated with an ESS. In [13–15], the ESS was sized for the WP plant to comply with the requirements of the grid codes. However, it seems that in many studies the ESS was sized for a combination of PV and wind power, not only for the WP. ESSs can also be used to improve the profitability of renewable energy power plants in the electricity market. For example, in [16], the utilization of the ESS of a virtual power plant was investigated to optimize trading in the electricity market. Frequently, studies investigating the sizing of an ESS for a PV–wind power system have included the economical aspect in the sizing algorithm—for example in [17–19]. However, as the main purpose of an ESS is to mitigate the fast power fluctuations of a PV–wind power plant, the temporal resolution of the measured or modelled generated power of the power plant should be very high. In [20], it was found that a sampling frequency of 10 Hz would be needed to sufficiently capture the fastest power fluctuations of a PV power plant. However, the temporal resolution of data utilized in many of the previous studies is generally significantly lower than 10 Hz. For example, the length of the data time step was 10 min in [14,17,18] and 1 min in [13].

The applied RR limit affects the sizing of an ESS for PV, wind, and PV–wind power plants. In [8–12], it was found that as the RR limit increased, the requirements for the ESS of a PV power plant decreased. The requirements for the ESS decreased because the higher applied RR limit allowed faster power fluctuations to be fed into the grid and thus less power fluctuation mitigation was needed by the ESS. Similar results were found in [21], where the ESS was sized for the whole power system of California by applying different RR limits. Based on these studies [8–12,21], the applied RR limit seems to have a more significant effect on the energy capacity of the ESS than on the power capacity of the ESS.

The size of the PV power plant also affects the sizing of the ESS. As the size of the PV power plant grows, the relative magnitude of the power fluctuations diminishes [5]. In [9,10], it was found that the required size for the ESS decreased relatively as the size of the PV power plant grew. For the WP plants, the relative magnitude of the power fluctuations decreased as the size of the wind farm grew [22]. In addition, as the size of the wind turbine rotor grew, the increased inertia of the rotor smoothed the power fluctuations [22]. It is expected that the size of the WP plant will also affect the required size for the ESS.

The objective of this study is to investigate how the applied RR limit affects the sizing of the ESS for RR control of PV and wind power plants and combined PV–wind power plants. The main novelty of this study is that, for the first time, the ESS requirements of wind and PV–wind power plants are compared comprehensively with various RR limits. The power and energy requirements and utilization rates of the ESS are studied utilizing modeled powers of PV and wind power plants based on a five-month period of operating

condition measurements carried out with a 10 Hz sampling frequency. The sizing of ESSs for wind and PV–wind power systems has not yet been studied with this high temporal resolution output power from the system. The lengths of the data time steps have been significantly longer for sizing the ESSs for wind [13,14] and PV–wind power [17,18] plants. It was found that as the applied RR limit increases, the capacity requirements for the ESSs of the PV, wind, and PV–wind power plants decrease. It was also found that as the size of the power plant grows, the energy and power capacity requirements for the ESS of a PV power plant decrease. However, the effect on energy capacity is very small. For the ESSs of wind and PV–wind power plants, the energy capacity requirement increases as the size of the power plant grows.

The article is composed as followings. First, the article presents the data used and the simulation methods of the power plants. Then, the results of the study are presented and compared to other studies. Lastly, further discussion and the conclusions of the study are presented.

2. Materials and Methods

2.1. Measurement Data

This study is based on the measurements conducted at the Tampere University Solar PV Power Station Research Plant in Finland [20]. The measured quantities for the PV power modeling were irradiance and PV module backside temperature. For the wind power modelling, the measured quantities were wind speed and ambient temperature. These four climatic measurement quantities were chosen because they are the main factors affecting the PV and wind power generation. In addition, with the climatic measurement data as the basis, this study is easier to replicate.

All the measurements were completed over a period of 153 days, the first day being 1 June 2019 and the last being 31 October 2019. The summer and early autumn months were chosen for the measurement period because the solar irradiance, and thus the magnitude of the PV power fluctuations, would otherwise be truly low. The wind speed is generally higher and fluctuates slightly more during the autumn and winter months in the Nordic countries [22]. However, the late autumn months and the winter months were not included in the measurement period because then the PV power production would be minimal. As the topic of this study was to investigate the size of ESS needed to mitigate the power fluctuations of a PV–wind power system, a high sampling frequency was needed to capture the fast fluctuations of irradiance and wind speed. A sampling frequency of 10 Hz was used in this study for all the measurements.

The irradiance measurements were completed with a photodiode-based Kipp&Zonen SPLite2 pyranometer mounted to a PV module located on the rooftop of the university building. The PV module faces nearly southwards and is mounted at a tilt angle of 45°, which is also the tilt angle of the pyranometer. The pyranometer used in this study was marked as S19 in [20]. This pyranometer was chosen because it would have least interactions with the shadows of buildings or trees. Along with the tilt angle of the PV module, the size and the nominal power of the PV module were used for PV power modeling. The nominal power of the PV module $P_{\text{nom, PV}}$ was 190 W. The length and the width of the PV module were 1475 mm and 986 mm, respectively. The backside temperature of the S19 PV module was measured with a National Instruments Pt100 temperature sensor.

The wind speed measurements were carried out with an ultrasonic VAISALA WS425 wind sensor. The wind sensor was mounted at the tip of the pole located at the highest point of the university building. The total height from the ground level to the wind sensor was 16.13 m. The ambient temperature was measured with a VAISALA HMP155 humidity and temperature sensor also located on the rooftop of the university building. The modeling of the PV and wind powers and the simulation of the RR-based control algorithm were carried out using MATLAB.

2.2. Experiment Formulation

The design process of the experimental research is presented as an activity diagram in Figure 1. First, the generated PV and wind powers were modeled for the different power plant sizes considering the main climatic parameters affecting the power generation. The applied RR limits determine the maximum RR level, which may cause the grid feed-in power of the power plants to fluctuate. The ESSs were sized so that all the power fluctuations are smoothed to the preferred level and the ESS has enough energy to maintain the grid feed-in power within the RR limit even during a sudden shutdown of the power plant.

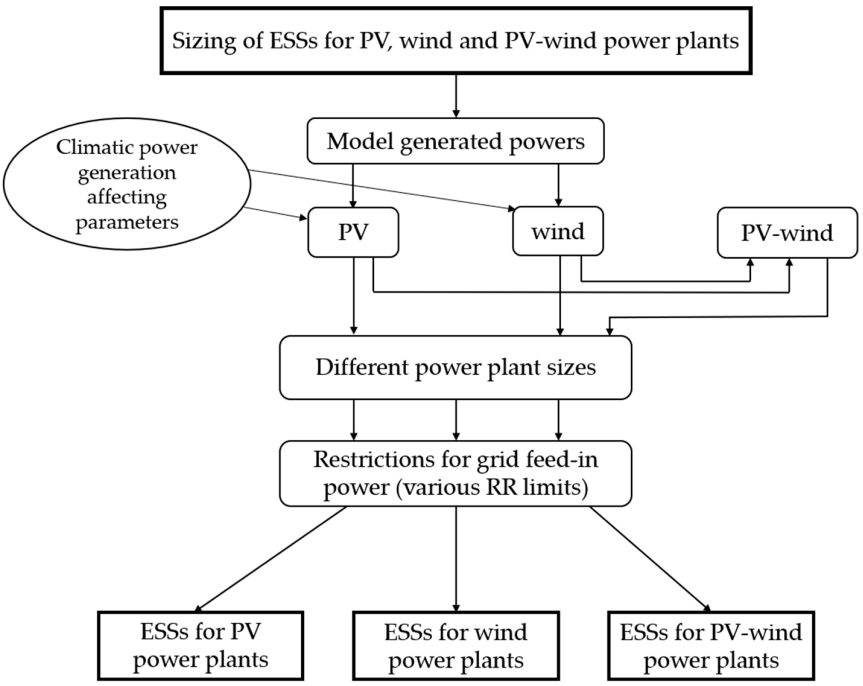

Figure 1. Activity diagram of the experimental research process.

2.3. PV and Wind Power Modeling

The PV power was modeled using measured irradiance and the backside temperature of the PV module. A spatial filter proposed in [23] was first applied to provide a more realistic irradiance exposure of a PV power plant, as the irradiance was measured from one sensor only. The filter simulated the output power smoothing effect as the spatial size of the PV power plant increased. The spatial irradiance $G_s(t)$ was calculated as

$$G_s(t) = \frac{G(t)}{\left(\frac{\sqrt{A_{PV}}}{2\pi \cdot 0.020}\right)s + 1} \quad (1)$$

where $G(t)$ is the measured irradiance, A_{PV} is the total area of the PV module array, and s is the Laplace transform variable. Because the A_{PV} is not just the area that the PV modules occupy but also the area between them, the space between the PV module rows needed to be calculated. The objective was to determine a suitable length for the empty space between the rows so that the PV modules would not shade each other during daytime in the summer months in Tampere, Finland. The length of the empty space was determined with a 20° angle of the altitude of the sun. Figure 2 illustrates the side view of the PV module rows and the empty space between them. The empty space between the PV module rows was determined with the minimum altitude angle of the sun during daytime in winter. As the minimum altitude angle of the sun is roughly 5° in Tampere, Finland, during daytime in winter, this led to the length of the empty space between the PV module rows being

determined as 7966 mm. With this empty space length, the land use of the PV power plant would be significantly larger than in typical PV power plants and economically unreasonable.

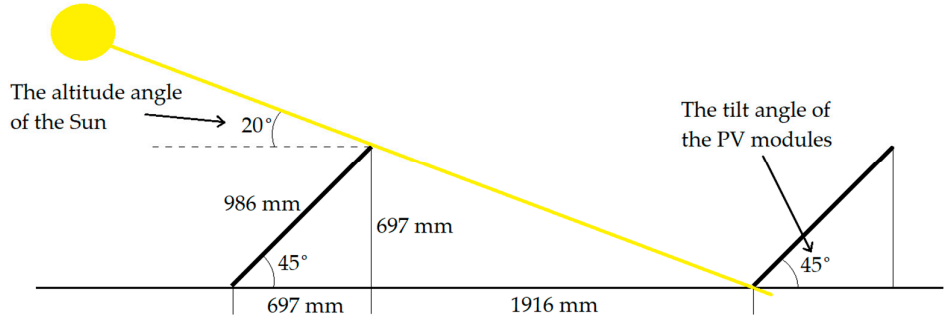

Figure 2. Illustration of the PV module rows and the space between them.

As seen in Figure 2, the empty space between the PV module rows was determined so that when the altitude angle of the Sun was 20°, the PV modules would not shade each other. Therefore, the length of the empty space was calculated to be 1916 mm. With this empty space length, the area that the PV modules occupied would be roughly 27% of the A_{PV}. This ratio is also called the packing factor. In [24], parameters of many different PV power plants were studied, and it was found that the packing factor value varied greatly. The packing factor values in [24] were between 30 and 90%, with a median value of 51%. As all the PV power plants studied in [24] were located farther south than the PV power plant in this study, the smaller packing factor was justified.

The generated PV power $P_{\text{gen, PV}}$ was simulated using a formula [25] that considers the effect of the PV module temperature T_{PVM} on the $P_{\text{gen, PV}}$ as

$$P_{\text{gen, PV}} = \frac{nP_{\text{nom, PV}}}{G_{\text{STC}}} G_{\text{S}}[1 - \beta(T_{\text{PVM}} - T_{\text{STC}})] \quad (2)$$

where n is the number of PV modules, G_{STC} is the irradiance in standard test conditions (STC), β is the temperature coefficient, and T_{STC} is the temperature in the STC. A value of 0.0045 1/°C was used for β, as this value was the average value in [25].

The basis for the WP modeling was the cubic WP equation and the air density equation. The air density ρ_{air} was calculated using an equation [26] that considers multiple climatic parameters. The ρ_{air} was calculated for each data point as

$$\rho_{\text{air}} = \frac{p_0}{R_{\text{air}} T_{\text{air}}} e^{\left(\frac{-gH}{R_{\text{air}} T_{\text{air}}}\right)} \quad (3)$$

where p_0 is the standard sea level atmospheric pressure (101,325 Pa), R_{air} is the specific gas constant for air (287.05 J/(kg·K)), T_{air} is the temperature of the air, g is the gravity constant (9.81 m/s^2), and H is the total altitude above sea level. The altitude above sea level for Tampere University, Tampere, is 140 m [27]. The applied value of H, 156.13 m, is the sum of the altitude of Tampere and the height of the modeled wind turbine (WT).

As the heights of the WTs were significantly higher than the height of the wind speed sensor from ground level, the measured wind speeds were extrapolated to the heights of the WTs. In Refs. [28,29], the wind speed power law was found to be sufficiently accurate at extrapolating wind speeds to given heights when using a suitable value for the shear exponent α. The power law was applied as

$$v_2 = v_1 \left(\frac{h_2}{h_1}\right)^{\alpha} \quad (4)$$

where v_2 is the extrapolated wind speed at height h_2, and v_1 is the measured wind speed at height h_1. The value for α would be 0.3 for a small town with some trees and 0.4 for a city area with tall buildings [28]. As the environment around the wind speed sensor of Tampere University has a few tall buildings but could be mainly considered a small town, the value of α was determined to be 0.35.

The preliminary wind turbine power $P_{\text{WT, pre}}$ was calculated as

$$P_{\text{WT, pre}}(v_2) = \begin{cases} 0, v_2 < v_{\text{cut-in}} \\ \frac{1}{2} A_{\text{swept}} \rho_{\text{air}} v_2^3 C_{\text{p}}, v_{\text{cut-in}} \leq v_2 < v_{\text{rated}} \\ P_{\text{rated,WT}}, v_{\text{rated}} \leq v_2 < v_{\text{cut-out}} \\ 0, v_{\text{cut-out}} \leq v_2 \end{cases} \quad (5)$$

where A_{swept} is the swept area of the WT rotor, C_{p} is the power coefficient of the WT, $P_{\text{rated, WT}}$ is the rated power of the WT, and $v_{\text{cut-in}}$, v_{rated}, and $v_{\text{cut-out}}$ are the cut-in, rated, and cut-out wind speeds of the WT, respectively. The WT starts generating power if the v_2 is at or higher than the $v_{\text{cut-in}}$. The WT stops generating power if v_2 is at or higher than $v_{\text{cut-out}}$. When v_2 is at v_{rated} or between v_{rated} and $v_{\text{cut-out}}$, the WT generates power at $P_{\text{rated, WT}}$. When v_2 is at $v_{\text{cut-in}}$ or between $v_{\text{cut-in}}$ and v_{rated}, the WT generates power according to the cubic WP equation [26]. The C_{p} values for the WTs needed to be calculated because the values were not available. The C_{p} value of a WT is dependent on the wind speed. However, according to [30], using a calculated maximum value of C_{p} as the constant value provides sufficient accuracy. The maximum C_{p} values were calculated for each WT using Equation (5).

As the wind speed measurements were carried out at a sampling frequency of 10 Hz, a low-pass filter was applied to take the inertia of the WT rotor into account and level the power fluctuations of $P_{\text{WT, pre}}$ to a more realistic level. A low-pass filter was used with WP modeling in [31,32]. The smoothed wind power $P_{\text{gen, WT}}$ was obtained by applying the first-order low-pass filter to $P_{\text{WT, pre}}$ as

$$P_{\text{gen, WT}}(t) = \frac{P_{\text{WT, pre}}(t)}{\tau_{\text{WT}} s + 1} \quad (6)$$

where τ_{WT} is the time constant of the WT. The low-pass filter smooths the power fluctuations to a more realistic level only if a suitable value is used for the time constant. If the time constant is too large, $P_{\text{gen, WT}}$ is oversmoothed and the effect of the power fluctuations decreases. The applied time constants for the WTs of this study were determined by comparing the time constant values to the values in Refs. [31,32] and the simulated power graphs visually to the measured power graphs in Refs. [33,34].

Various power plant sizes were considered to study how the size of the power plant affects the size of the ESS. The nominal powers of the considered combined PV–wind power plants were 20 kW, 400 kW, 2 MW, and 6 MW. These nominal powers were chosen because they would show the effects of small- and medium-scale power plants on the sizing of ESSs. A total of 50% of the total nominal power consisted of PV power and 50% WP. The parameter values of these combined PV–wind power plants are presented in Table 1. The separate PV and wind power plants were simulated using the same values. The nominal powers of these separate power plants were 10 kW, 200 kW, 1 MW, and 3 MW. The nominal power of the PV power system was scaled using different numbers of PV modules. The nominal power of the WP system was scaled using four different WT models. The WT models used in this study were the E-10 10 kW WT produced by Ryse Energy [35], the D2CF 200 kW WT produced by Aeolia Windtech [36], the E-58/10.58 1 MW WT produced by Enercon [37], and the E-82 E3 3 MW WT produced by Enercon [38].

Table 1. Parameter values of the studied PV–wind power plants.

Total Nominal Power	**20 kW**	**400 kW**	**2 MW**	**6 MW**
Nominal PV power	10 kW	200 kW	1 MW	3 MW
Number of PV modules	53	1053	5263	15,789
PV module array area	149 m^2	2957 m^2	14,780 m^2	44,340 m^2
Rated wind power	10 kW	200 kW	1 MW	3 MW
Wind turbine height	16.5 m	40.3 m	70.5 m	98 m
Swept area	75.4 m^2	650 m^2	2697 m^2	5281 m^2
Calculated power coefficient	0.48	0.44	0.43	0.50
Time constant	15 s	23 s	30 s	40 s
Cut-in wind speed	2 m/s	3 m/s	2.5 m/s	3 m/s
Rated wind speed	9 m/s	10.9 m/s	12 m/s	16 m/s
Cut-out wind speed	30 m/s	20 m/s	34 m/s	34 m/s

2.4. ESS Control Strategy

The simulation model contained the power plant and the ESS. An illustration of the system is presented in Figure 3. The power generated by the power plant P_{gen} equals the sum of the power fed to the grid P_{grid} and the charging power of the ESS P_{ESS} as $P_{gen} = P_{grid} + P_{ESS}$. The inverter, ESS, and power line losses were not taken into account. The goals for the ESS were to mitigate the power fluctuations of the P_{gen} to a preferred level and to make sure that at every moment the ESS had enough energy in case of a sudden shutdown of the power plant.

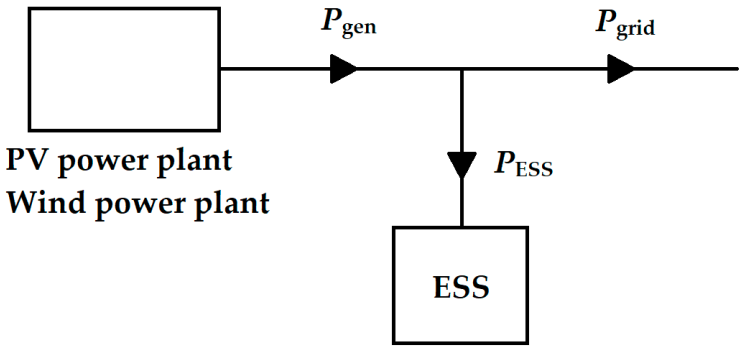

Figure 3. Diagram of the power system model.

The control algorithm of the ESS was an RR-based control algorithm. The same algorithm was used in [8]. The control algorithm operated so that the power RR of the power fed to the grid RR_{grid} never exceeded the applied power RR limit RR_{lim} as

$$\left|RR_{grid}\right| \leq RR_{lim} \tag{7}$$

where the RR_{grid} was calculated by dividing the difference of the power values of two consecutive time steps by the time difference of the time steps. In order to comply with the applied RR limit even during a sudden shutdown of the power plant, the minimum energy level of the ESS $E_{ESS,\,min}$ at every moment was

$$E_{ESS,\,min} = \frac{{P_{grid}}^2}{2 \cdot RR_{lim}} \tag{8}$$

The energy level of the ESS was kept as close to $E_{ESS,\,min}$ as possible by discharging the ESS whenever possible. The applied RR limits were 1, 2, 3, 5, 7, 10, 13, 15, 17, and 20%/min.

An example of the operation of the control algorithm with different applied RR limits is presented in Figure 4. As seen in Figure 4a, the P_{grid} stayed within the RR limit as the ESS

mitigated the fastest power fluctuations by charging or discharging power when needed. Figure 4b presents the P_{grid} when different RR limits were applied. The P_{grid} remained significantly smoother when the RR limit of 1%/min was applied compared to the two less strict RR limits, and even the least strict RR limit of 20%/min smoothened the power fluctuations considerably.

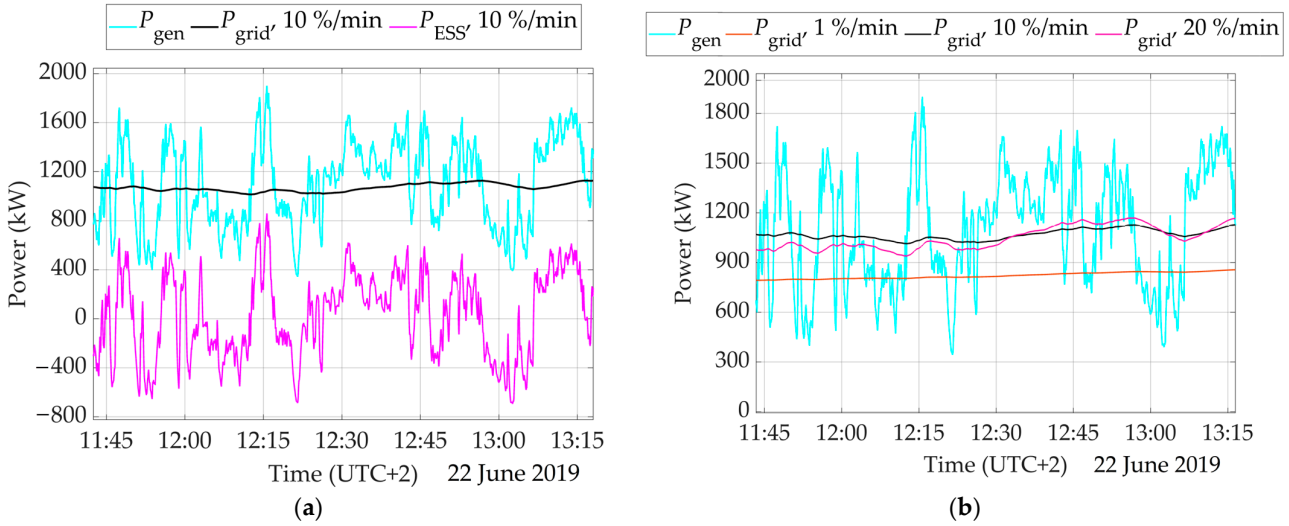

Figure 4. (**a**) Power generated by the 2 MW PV–wind power plant, power fed to the grid, and power of the ESS with an RR limit of 10%/min during a period of high fluctuation. (**b**) Power generated by the 2 MW PV–wind power plant and power fed to the grid while applying different RR limits during the same period.

3. Results

The results of this study were divided into two categories. In Section 3.1, the power and energy requirements of the ESSs are presented. In Section 3.2, the utilization rates of the ESSs are presented. In both subsections, the results of the separate PV and wind power plants are presented before the results of the combined PV–wind power plants.

3.1. Power and Energy Requirements of the ESSs

Figure 5 presents the relative energy and power capacities of the ESSs required for the PV power plants as a function of the applied RR limit. In Figure 5a, it can be seen that as the RR limit increased, the relative energy capacities of the ESSs decreased significantly, which was expected, as the need to mitigate the power fluctuations decreased as the RR limit increased. On clear-sky days, the required energy capacity of the ESS was the highest $E_{ESS,\,min}$ value, which was determined by the highest P_{grid} value, as stated in Equation (8). As the size of the PV power plant increased, the relative energy capacities of the ESSs decreased a tiny amount. This effect is not clearly visible in Figure 5a, as the difference in the values of the largest and the smallest PV power plant was only 0.6% on average. The reason for this is that the highest production power of the PV power plant increased nearly linearly as the size of the PV power plant increased; thus, the relation stayed practically the same. This phenomenon was also detected also in [9,10], but the difference in the relative energy capacities of the ESSs was notably greater between the different PV power plant sizes due to differences in the ESS control algorithm. The relative energy capacity values of the ESSs of this study were generally notably higher compared to the values in [8–11]. The difference in the relative energy capacity values of the ESSs can be explained with the use of different control algorithms in Refs. [9–11]. As the control algorithm in [8] was the same as the one used in this study, the difference was caused by the fact that the generated power of the PV power plant was based on measured power in [8], not on modeled PV

power as in this study. The relative energy capacity values of the ESSs in [12] match the values of this study well, however.

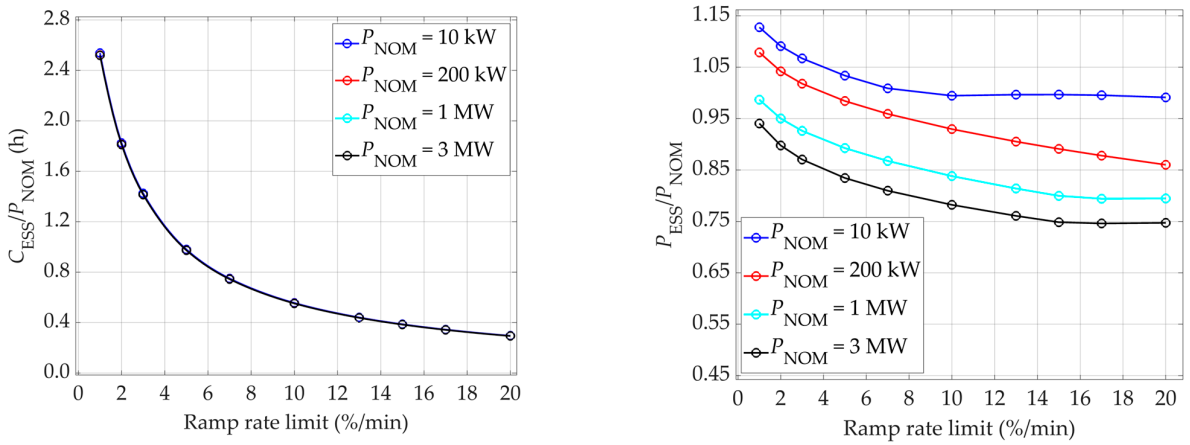

Figure 5. Required relative energy (**a**) and power (**b**) capacities of the ESSs of the PV power plants as a function of the RR limit.

In Figure 5b, the relative power capacities of the ESSs decreased as the RR limit increased. There is a clear difference between the relative power capacity values of the ESSs of the different PV power plant sizes. The difference in the values was greater for the higher RR limits than for the lower RR limits. With the three largest RR limits, the relative power capacity values of the ESS of the largest PV power plant were roughly 22% smaller than the values of the smallest PV power plant. The reason for the decreasing relative power capacity requirement of the ESS as the size of the PV power plant grows is the diminishing relative magnitude of the power fluctuations with increasing plant size. As the fastest power fluctuations decrease, relatively less ESS power is needed to mitigate them. This smoothing effect was also detected in [5,9,10]. The relative power capacity values of the ESSs in this study were very similar to the values in [8–12] when comparing the values of similar nominal power PV power plants. For example, at the applied RR limit of 10%/min, the relative power capacity values of the ESSs in this study were roughly 93%, 84%, and 78% for the nominal powers of the PV power plants of 200 kW, 1 MW, and 3 MW, respectively. At the applied RR limit of 10%/min, the relative power capacity values of the ESSs were roughly 76–84% in [9], 72–88% in [10], 71% in [11], and 72–86% in [12] for the nominal powers of the PV power plants of between roughly 100 kW and 7 MW.

In Figure 5b, the required power capacity of the ESS was higher than the nominal power of the power plant with RR limits of up to 7 and 3%/min for the 10 kW and 200 kW PV power plants, respectively. The reason for this is the cloud enhancement phenomenon [39]. In the cloud enhancement phenomenon, G is higher than G_{STC}, and thus, the PV power plant is able to generate more power than the nominal power of the power plant. If fast power fluctuations happen during the cloud enhancement phenomenon, the required P_{ESS} can be higher than the nominal power of the PV power plant. These occasions happened on five days for the 10 kW PV power plant and on three days for the 200 kW PV power plant during the measurement period. The required power of the ESS was not found to be higher than the nominal power of the PV power plant in studies [8–12].

Figure 6 presents the required relative energy and power capacities of the ESSs of the WP plants as a function of the applied RR limit. In Figure 6a, it can be seen that as the RR limit increased, the relative energy capacities of the ESSs of the WP plants decreased significantly. It is also visible that the larger the WP plant was, the higher the relative ESS energy capacities were. However, the relative energy capacity values of the ESSs of the 10 kW and 200 kW WP plants were practically the same for all RR limits. These values were also practically the same between the 1 MW and 3 MW WP plants when the RR limit

was roughly 7%/min or higher. However, there was a clear difference when comparing the values of the 10 kW and 200 kW WP plants to the values of the 1 MW and 3 MW WP plants. This difference was more notable at the lower RR limit values. This effect can be explained by the height of the WT. As the height of the WT increased, the energy density of the wind increased. This means that there was more power to be extracted for the WT, and thus, the P_{grid} was also generally higher. With the generally higher P_{grid}, the relative energy capacity of the ESS also needed to be higher in case of a possible sudden shutdown of the power plant. With the three smallest RR limits, the relative energy capacity values of the ESS of the largest WP plant were roughly 82% higher than the values of the smallest WP plant.

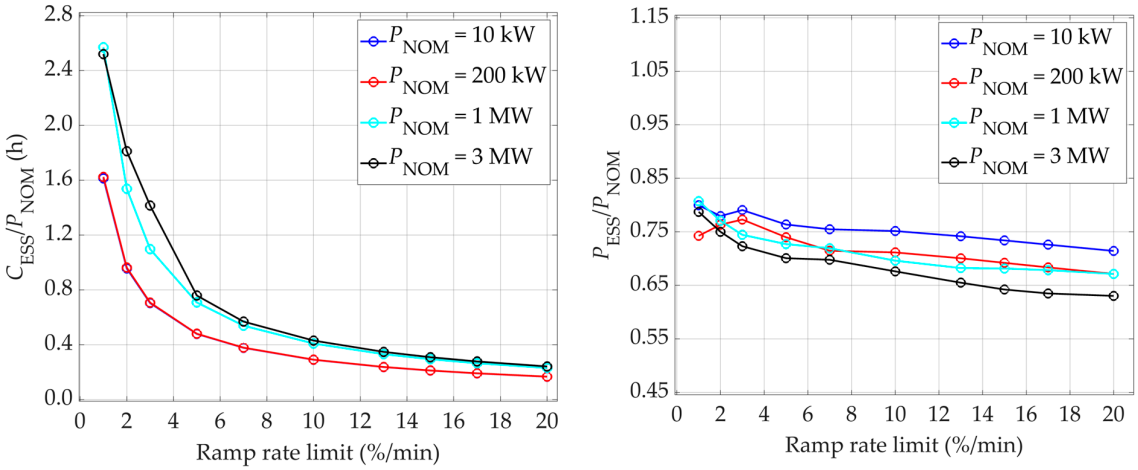

Figure 6. Required relative energy (**a**) and power (**b**) capacities of the ESSs of the wind power plants as a function of the RR limit. The blue line and the red line in (**a**) are on top of each other.

In Figure 6b, the values of the relative power capacities of the ESSs of the WP plants generally decreased as the RR limit increased. As the size of the WP plant increased, the relative power capacities of the ESSs generally decreased because the relative magnitude of the power fluctuations of the WP plant decreased. The relative magnitude of the power fluctuations decreased as the inertia of the WT rotor increased with increasing WT size [40]. However, as the RR limit increased from 1%/min to 3%/min, the relative power capacity of the ESS of the 200 kW WP plant increased. The reasons for this are covered in Section 4.

Figure 7 presents the relative energy and power capacities of the ESSs required for the PV–wind power plants. In Figure 7a, it can be seen that as the RR limit increased, the relative energy capacities of the ESSs decreased significantly. The difference between the relative energy capacity values of the ESSs of different power plant sizes was small when the RR limit was 10%/min or higher. The difference in these values was more noticeable with stricter RR limits. With the three smallest RR limits, the relative energy capacity values of the ESS of the largest power plant were roughly 24% higher than the values of the smallest power plant. The increase in the relative energy capacity values as the size of the PV–wind power plant increased was reasonable since the larger wind turbine had a greater effect on increasing the values than the larger PV power plant had on lowering the values, as seen in Figures 6a and 5a, respectively.

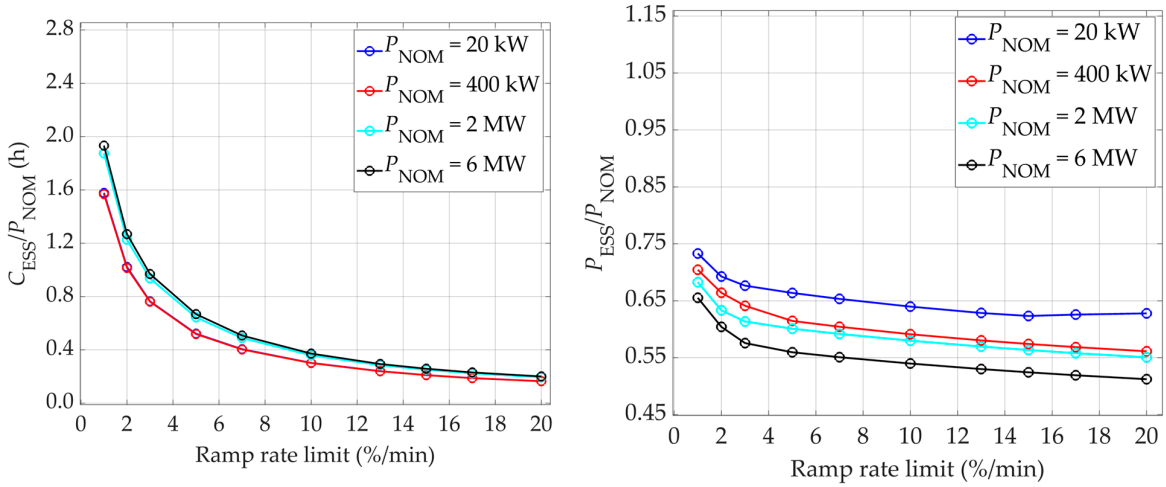

Figure 7. Required relative energy (**a**) and power (**b**) capacities of the ESSs of the PV–wind power plants as a function of the RR limit. The blue line and the red line in (**a**) are on top of each other.

In Figure 7b, it can be seen that as the RR limit increased, the relative power capacity requirements of the ESSs decreased. The effect of the decreasing required size of the ESS as the RR limit increased was less significant on the relative power capacity than on the relative energy capacity (Figure 7a). With the relative power capacities of the ESSs, the difference in the values between the different power plant sizes increased as the RR limit increased. With the three largest RR limits, the relative power capacity values of the ESS of the largest power plant were roughly 17% smaller than the values of the smallest power plant. The relative power capacity values of the ESS of the PV–wind power plant decreased as the size of the power plant increased because the increasing PV plant size and WT size both decreased the relative magnitude of the power fluctuations and thus the need for power smoothing, as seen in Figures 5b and 6b, respectively.

Figure 8 presents various percentiles of the required relative daily energy and power capacities of the ESS of the 2 MW PV–wind power plant as a function of the RR limit. The values of the 50th percentile of the relative daily energy and power capacity requirements were roughly 50% and 60% of the values of the 100th percentile, respectively. When comparing the 90th and the 100th percentiles, the relative daily energy and power capacity values of the 90th percentile were both roughly 80% of the values of the 100th percentile. These findings show that for most days, the energy and power capacity of the ESS of the 2 MW PV–wind power plant could have been significantly smaller than the size required to mitigate all the power fluctuations of the measurement period. Similar findings were observed in [8] with a small PV power plant.

Table 2 presents the required energy and power capacities of the ESSs of the power plants with the applied RR limit of 10%/min. For the nominal powers of 10 kW and 200 kW, the required energy capacities of the ESSs of the WP plants were roughly 48% smaller than the values of the ESSs of the PV power plants. For the nominal powers of 1 MW and 3 MW, the required energy capacities of the ESSs of the WP plants were roughly 24% smaller than the values of the PV power plants. For the required power capacity of the ESS, the difference was smaller. The required power capacity values of the ESSs of the WP plants were roughly 24% and 15% smaller than the values for the PV power plants for the two smaller and the two larger nominal powers, respectively.

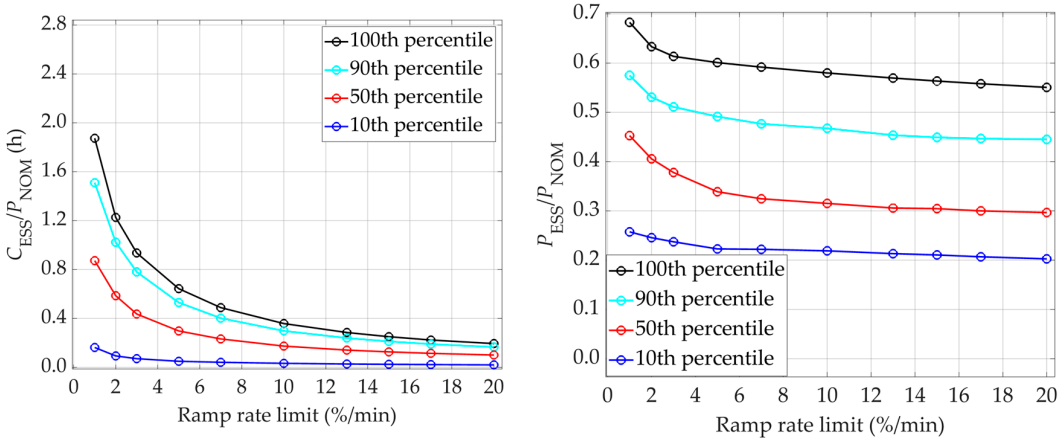

(**a**) (**b**)

Figure 8. Percentiles of the required relative daily energy (**a**) and power (**b**) capacities of the ESS of the 2 MW PV–wind power plant as a function of the RR limit.

Table 2. Required energy and power capacities of the ESSs of the power plants with the applied RR limit of 10%/min.

Power Plant	Nominal Power (kW)	Energy Capacity (kWh)	Power Capacity (kW)
PV	10	5.567	9.946
	200	110.6	185.9
	1000	553.4	838.4
	3000	1657	2347
Wind	10	2.904	7.514
	200	58.25	142.3
	1000	409.3	696.2
	3000	1291	2028
PV–wind	20	6.043	12.80
	400	120.2	236.5
	2000	717.2	1160
	6000	2232	3239

As the nominal power values of the PV–wind power plants were twice the values of the PV and the wind power plants, the sizing requirements for the ESSs cannot be compared with the direct values. Comparing the graphs of Figures 5a and 7a at the RR limit of 10%/min, the required relative energy capacities of the ESSs of the PV–wind power plants were roughly 40% smaller than for the PV power plants. When comparing the graphs of Figures 6a and 7a at the RR limit of 10%/min, the required relative energy capacities of the ESSs of the PV–wind power plants were roughly 3% larger and 13% smaller than for the WP plants for the two smaller and the two larger nominal powers, respectively. For the required relative power capacities of the ESSs at the RR limit of 10%/min, the values of the PV–wind power plants were roughly 33% and 17% smaller than the values of the PV and the wind power plants, respectively.

3.2. Utilization Rate of the ESSs

The daily maximum shares of energy cycled through the ESSs of PV and wind power plants are presented in Figure 9. In Figure 9a, it can be seen that the values for the PV power plants decreased significantly as the RR limit increased. This behavior is in line with the results of [8], although the shares obtained herein were somewhat higher. There was only a tiny visible difference between the values of the different power plant sizes. The values

decreased slightly as the amount of PV power grew. This was caused by the smoothing effect on the power fluctuations of the larger PV power plant [5].

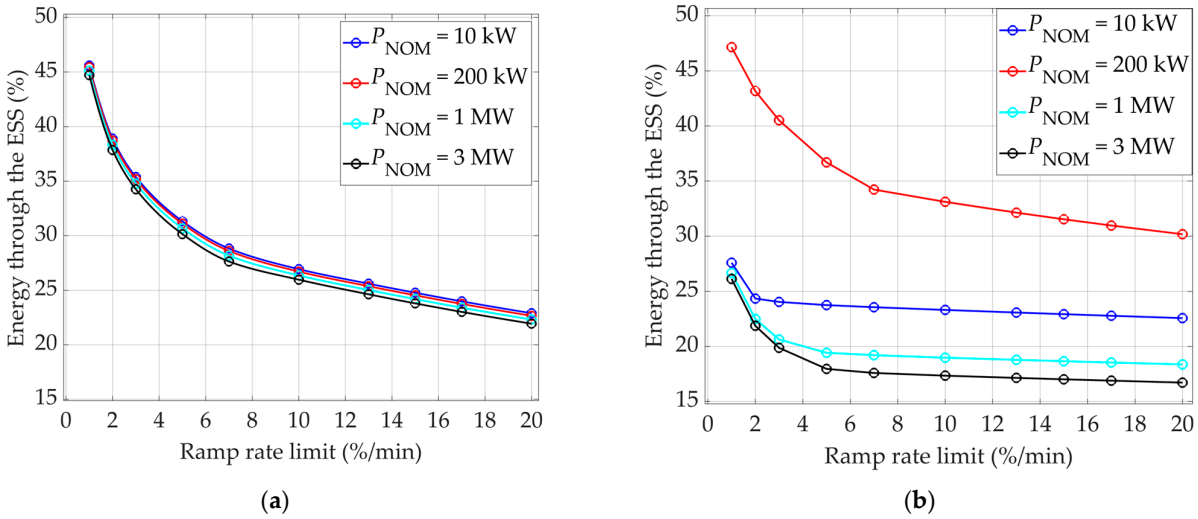

Figure 9. Daily maximum shares of energy cycled through the ESSs of the PV power plants (**a**) and the wind power plants (**b**) as a function of the RR limit.

In Figure 9b, it can be seen that the daily maximum shares of energy cycled through the ESSs of the WP plants decreased as the RR limit increased. Without taking the values of the 200 kW WP plant into account, the daily maximum shares of energy cycled through the ESSs also decreased as the size of the WP plant increased because the power fluctuations diminished as the inertia of the WT rotor increased. The daily maximum share of energy cycled through the ESS of the 200 kW WP plant also decreased as the RR limit increased, but the values were clearly higher than the values of the other WP plants. The reasons for this are covered in Section 4.

Figure 10 presents the daily maximum shares of energy cycled through the ESSs of the PV–wind power plants and the percentiles of the shares of energy cycled daily through the ESS of the 2 MW PV–wind power plant. It can be seen in Figure 10a,b that the daily shares of cycled energy decreased notably as the RR limit increased. This was caused by the decreased need to level the power fluctuations with the higher RR limits. In Figure 10a, the daily maximum shares also generally decreased when the size of the power plant increased. The values of the 50th and 90th percentile were roughly 70% and 85% of the values of the 100th percentile, respectively. This means that the ESS would need to operate significantly more on a highly fluctuating day than on an average day. This also applies for the separate PV and wind power plants. Similar findings with an ESS of a small PV power plant were observed in [8].

Table 3 presents the daily maximum values of the time the ESS charged and discharged for RR limits of 1, 10, and 20%/min for the 2 MW PV–wind power plant. The differences between the RR limits were higher for charging than for discharging. The charging and discharging times did not decrease as significantly as the daily maximum shares of energy cycled through the ESS when the RR limit increased. This means that the ESS of the PV–wind power system seemed to operate for an almost equally long time with different RR limits, but the amount of energy charged or discharged varied more notably, as seen in Figure 10a. The applied control algorithm controlled the ESS to operate almost all the time to be prepared for a sudden shutdown of the power plant.

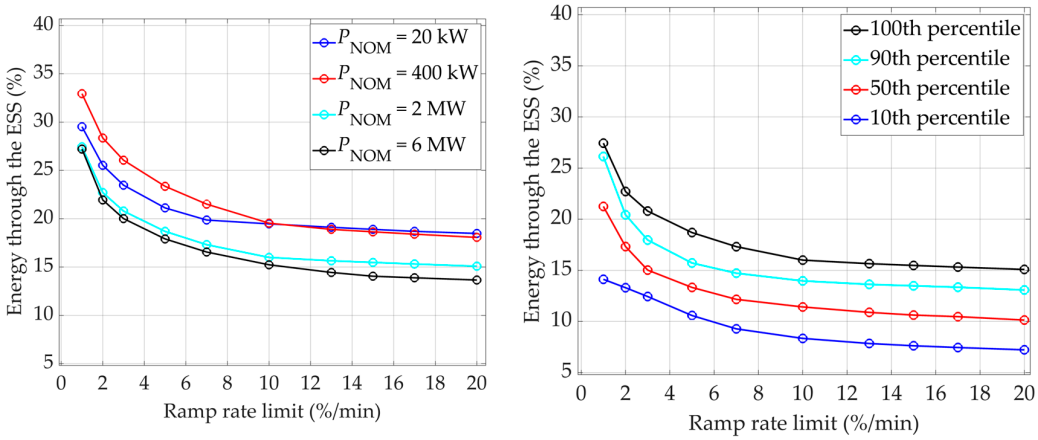

Figure 10. Daily maximum shares of energy cycled through the ESSs of the PV–wind power plants (**a**) and percentiles of daily shares of energy cycled through the ESS of the 2 MW PV–wind power plant (**b**) as a function of the RR limit.

Table 3. Daily maximum values of the time the ESS charged and discharged for RR limits of 1, 10, and 20%/min for the 2 MW PV–wind power plant.

	RR 1%/min	**RR 10%/min**	**RR 20%/min**
Time ESS charged (%)	61.1	56.5	55.1
Time ESS discharged (%)	60.6	59.6	59.0

4. Discussion

The mathematical models of PV and wind power plants used were based on multiple studies and considered all main climatic parameters that would affect the power generation of the power plants. However, the choices and simplifications done in the modelling affected the results. Particularly with the WP modeling, the chosen WT models and the determined time constants for the WTs had an effect on the results. The WT models [35–38] were chosen for this study because their nominal powers were suitable and there were enough detailed data available about these WTs. As there were no time constants available for the WTs, the suitable values for the time constants of the WTs needed to be determined by visually comparing the simulated power graphs of the WTs to the measured power graphs in Refs. [33,34]. Because the time constant values in Refs. [31,32] were used in those studies for the output power smoothing of the WP plants and not on the modeling of realistic wind power, the values were not used in this study directly. The use of too large time constants would have suppressed the WP fluctuations.

The reason why the daily maximum shares of energy cycled through the ESS were significantly higher for the 200 kW WP plant than for the other WP plants in Figure 9b is that $v_{\text{cut-out}}$ and the gap between v_{rated} and $v_{\text{cut-out}}$ were clearly smaller for the 200 kW WT than for the other WTs, as seen in Table 1. Thus, the 200 kW WT would have stopped generating power at lower wind speeds than the other WTs. In addition, the share of power generated at its P_{rated} was smaller than for the other WTs. This means that the share of power generated at power other than the P_{rated} was larger for the 200 kW WP plant than for the other WP plants. Because the share of fluctuating power production was larger, the ESS was needed more often to level the power fluctuations. That is why the amount of energy cycled through the ESS of the 200 kW WP plant was significantly higher than for the other WP plants, as shown in Figure 9b.

The significantly smaller $v_{\text{cut-out}}$ of the 200 kW WT also explains why the required relative power capacity of its ESS differed from the values of the ESSs of the other WTs at the applied RR limit of 1%/min in Figure 6b. During a high ramp up of wind speed, the $v_{\text{cut-out}}$

of the 200 kW WT was exceeded first, and thus the 200 kW WT stopped generating power first among the WTs. Because the 200 kW WT stopped generating power relatively quickly compared to the other WTs, the $P_{\text{gen, WT}}$ of the 200 kW WP plant did not rise relatively as high as the $P_{\text{gen, WTs}}$ of the other WTs during a high ramp up of wind speed. This means that the difference between the $P_{\text{gen, WT}}$ and the P_{grid} of the 200 kW WT was the smallest among the WTs during a high ramp up of wind speed. Because this difference was the amount of power that the ESS needed to charge, the required relative power capacity of the ESS of the 200 kW WT was the smallest for the RR limit of 1%/min. This effect was small, and practically noticeable only at the RR limit of 1%/min, as the P_{grid} then varied significantly more slowly than with the other applied RR limits. The power generation affecting parameters of WTs can vary a lot in practice, as seen in this study, especially with the $v_{\text{cut-out}}$ values of the WTs. Because these parameters can affect the sizing of an ESS for a WP plant relatively strongly, the effect of the power plant size on the size of the ESS is more ambiguous with the WP plants than with the PV power plants.

Future research directions include using measured power data of PV and wind power plants for the sizing of ESSs. Those results could then be compared with the ones obtained based on simulated powers. In addition, the economic point of view could be included in the study while still keeping the investigation of the power fluctuations comprehensive. As the results of this study show, most of the time a smaller-sized ESS would be sufficient at keeping the power fluctuations of a 2 MW PV–wind power plant within the applied RR limits. Thus, it would not likely be economically optimal to size the ESS of a PV–wind power plant to mitigate even the fastest power fluctuations.

5. Conclusions

This article presented a comprehensive study on the sizing of ESSs for PV, wind, and PV–wind power plants when different RR limits were applied. The study was conducted based on climatic measurements carried out with a 10 Hz sampling frequency for a period of 153 days. The modelling of the PV and wind power was based on multiple studies and took into account the main climatic parameters that would affect the PV and wind power generation. Therefore, using high temporal resolution for the generated powers, the sizing of the ESSs in this study was able to consider even the fastest power fluctuations of PV and wind power. The main sizing qualities were the relative energy and power capacities of the ESS and the shares of energy cycled through the ESS.

It was found that the applied RR limit significantly affected the required energy capacities of the ESSs of PV, wind, and PV–wind power plants, which was expected based on the previous research. The applied RR limit moderately affected the required power capacities and utilization rates of the ESSs for the PV, wind, and PV–wind power plants, which was also in line with previous studies. The energy and power capacity requirements for the ESS of the PV power plant decreased when the size of the PV power plant grew. These results are also in line with previous studies considering ESS sizing for PV power plants. For the wind and PV–wind power plants, the required energy capacity of the ESS increased and the required power capacity decreased when the size of the WP plant grew. This was expected, as the larger WTs would face wind that has a higher energy density, and the increased inertia of the WT rotor would smooth the power fluctuations.

Although the results of this study related to the sizing of ESSs for PV power plants are in line with previous studies, the results of the sizing of ESSs for wind and PV–wind power plants are novel. The novelty and the value of this study are that the results can be used for sizing ESSs for wind or PV–wind power plants to comply with different applied RR limits. However, as the ESSs of this study were sized so that they could mitigate even the fastest power fluctuations of PV and wind power, ESSs of this size would probably not be economically reasonable.

Author Contributions: Conceptualization, M.T. and K.L.; methodology, M.T.; formal analysis, M.T.; writing—original draft preparation, M.T.; writing—review and editing, K.L. and T.R.; supervision, K.L. All authors have read and agreed to the published version of the manuscript.

Funding: This research was funded by Business Finland, grant number 1191/31/2022. K. Lappalainen was funded by the Academy of Finland, grant number 348701.

Data Availability Statement: The data presented in this study are available on request from the corresponding author.

Conflicts of Interest: The authors declare that they have no known competing financial interests or personal relationships that could have appeared to have influenced the work reported in this paper.

Nomenclature

A_{PV}	area of the PV module array (m^2)
A_{swept}	swept area of a WT (m^2)
α	wind shear exponent
β	temperature coefficient of the PV module
C_p	power coefficient of a WT
$E_{ESS,\,min}$	minimum energy level of the ESS (J)
g	gravity constant (m/s^2)
G	measured irradiance (W/m^2)
Gs	spatially smoothed irradiance (W/m^2)
Gs_{TC}	irradiance in STC (W/m^2)
H	altitude above sea level (m)
h_1	wind speed measurement height (m)
h_2	wind speed extrapolated height (m)
n	number of PV modules
P_{ESS}	power of the ESS (W)
P_{gen}	generated power of a power plant (W)
$P_{gen,\,PV}$	generated PV power (W)
$P_{gen,\,WT}$	generated wind power (W)
P_{grid}	power fed to the grid (W)
$P_{nom,\,PV}$	nominal power of the PV module (W)
$P_{rated,\,WT}$	rated power of a WT (W)
$P_{WT,\,pre}$	preliminary power of a WT (W)
p_0	sea level atmospheric pressure (Pa)
R_{air}	specific gas constant of air (J/(kg·K))
RR_{grid}	ramp rate of grid input power (W/s)
RR_{lim}	ramp rate limit (W/s)
ρ_{air}	density of air (kg/m^3)
s	Laplace transform variable
T_{air}	temperature of air (K)
T_{PVM}	backside temperature of the PV module (°C)
T_{STC}	temperature of STC (°C)
τ_{WT}	time constant of a WT (s)
$v_{cut\text{-}in}$	cut-in wind speed of a WT (m/s)
$v_{cut\text{-}out}$	cut-out wind speed of a WT (m/s)
v_{rated}	rated wind speed of a WT (m/s)
v_1	measured wind speed (m/s)
v_2	extrapolated wind speed (m/s)
Abbreviations	
ESS	energy storage system
PV	photovoltaic
RR	ramp rate
STC	standard test conditions
WP	wind power
WT	wind turbine

References

1. How Rapidly Will the Global Electricity Storage Market Grow by 2026? Available online: https://www.iea.org/articles/how-rapidly-will-the-global-electricity-storage-market-grow-by-2026 (accessed on 14 May 2023).
2. European Commission. *Energy Storage—Underpinning a Decarbonised and Secure EU Energy System*; Commission Staff Working Document: Brussels, Belgium, 2023; Available online: https://energy.ec.europa.eu/topics/research-and-technology/energy-storage/recommendations-energy-storage_en (accessed on 14 May 2023).
3. Martins, J.; Spataru, S.; Sera, D.; Stroe, D.-I.; Lashab, A. Comparative Study of Ramp-Rate Control Algorithms for PV with Energy Storage Systems. *Energies* **2019**, *12*, 1342. [CrossRef]
4. Lappalainen, K.; Valkealahti, S. Experimental study of the maximum power point characteristics of partially shaded photovoltaic strings. *Appl. Energy* **2021**, *301*, 117436. [CrossRef]
5. Marcos, J.; Marroyo, L.; Lorenzo, E.; Alvira, D.; Izco, E. Power output fluctuations in large scale PV plants: One year observations with one second resolution and a derived analytic model. *Prog. Photovolt. Res. Appl.* **2011**, *19*, 218–227. [CrossRef]
6. Parsons, B.K.; Wan, Y.; Kirby, B. Wind Farm Power Fluctuations, Ancillary Services, and System Operating Impact Analysis Activities in the United States. In Proceedings of the European Wind Energy Conference, Copenhagen, Denmark, 2–6 July 2001.
7. Gevorgian, V.; Booth, S. *Review of PREPA Technical Requirements for Interconnecting Wind and Solar Generation*; National Renewable Energy Laboratory (NREL): Golden, CO, USA, 2013. [CrossRef]
8. Lappalainen, K.; Valkealahti, S. Sizing of energy storage systems for ramp rate control of photovoltaic strings. *Renew. Energy* **2022**, *196*, 1366–1375. [CrossRef]
9. Schnabel, J.; Valkealahti, S. Energy Storage Requirements for PV Power Ramp Rate Control in Northern Europe. *Int. J. Photoenergy* **2016**, *2016*, 2863479. [CrossRef]
10. Schnabel, J.; Valkealahti, S. Compensation of PV Generator Output Power Fluctuations with Energy Storage Systems. In Proceedings of the 31st European Photovoltaic Solar Energy Conference and Exhibition, Hamburg, Germany, 14–18 September 2015. [CrossRef]
11. Makibar, A.; Narvarte, L.; Lorenzo, E. On the relation between battery size and PV power ramp rate limitation. *Sol. Energy* **2017**, *142*, 182–193. [CrossRef]
12. Marcos, J.; Storkël, O.; Marroyo, L.; Garcia, M.; Lorenzo, E. Storage requirements for PV power ramp-rate control. *Sol. Energy* **2014**, *99*, 28–35. [CrossRef]
13. Tadie, A.T.; Guo, Z.; Xu, Y. Hybrid Model-Based BESS Sizing and Control for Wind Energy Ramp Rate Control. *Energies* **2022**, *15*, 9244. [CrossRef]
14. Brekken, T.K.A.; Yokochi, A.; von Jouanne, A.; Yen, Z.Z.; Hapke, H.M.; Halamay, D.A. Optimal Energy Storage Sizing and Control for Wind Power Applications. *IEEE Trans. Sustain. Energy* **2011**, *2*, 69–77. [CrossRef]
15. Wang, W.; Mao, C.; Lu, J.; Wang, D. An Energy Storage System Sizing Method for Wind Power Integration. *Energies* **2013**, *6*, 3392–3404. [CrossRef]
16. Li, B.; Ghiasi, M. A New Strategy for Economic Virtual Power Plant Utilization in Electricity Market Considering Energy Storage Effects and Ancillary Services. *J. Electr. Eng. Technol.* **2021**, *16*, 2863–2874. [CrossRef]
17. Zhang, N.; Yang, N.-C.; Liu, J.-H. Optimal Sizing of PV/Wind/Battery Hybrid Microgrids Considering Lifetime of Battery Banks. *Energies* **2021**, *14*, 6655. [CrossRef]
18. Al-Shereiqi, A.; Al-Hinai, A.; Albadi, M.; Al-Abri, R. Optimal Sizing of Hybrid Wind-Solar Power Systems to Suppress Output Fluctuation. *Energies* **2021**, *14*, 5377. [CrossRef]
19. Geem, Z.W. Size optimization for a hybrid photovoltaic–wind energy system. *Electr. Power Energy Syst.* **2012**, *42*, 448–451. [CrossRef]
20. Torres Lobera, D.; Mäki, A.; Huusari, J.; Lappalainen, K.; Suntio, T.; Valkealahti, S. Operation of TUT Solar PV Power Station Research Plant under Partial Shading Caused by Snow and Buildings. *Int. J. Photoenergy* **2013**, *2013*, 837310. [CrossRef]
21. Headley, A.J.; Copp, D.A. Energy storage sizing for grid compatibility of intermittent renewable resources: A California case study. *Energy* **2020**, *198*, 117310. [CrossRef]
22. Nørgård, P.; Giebel, G.; Holttinen, H.; Söder, L.; Petterteig, A. Fluctuations and Predictability of Wind and Hydropower. Deliverable 2.1. Forskningscenter Risoe, Risoe-R, Denmark. 2004. Available online: https://orbit.dtu.dk/en/publications/fluctuations-and-predictability-of-wind-and-hydropower-deliverabl (accessed on 14 May 2023).
23. Marcos, J.; Marroyo, L.; Lorenzo, E.; Alvira, D.; Izco, E. From irradiance to output power fluctuations: The pv plant as a low pass filter. *Prog. Photovolt. Res. Appl.* **2011**, *19*, 505–510. [CrossRef]
24. Ong, S.; Campbell, C.; Denholm, P.; Margolis, R.; Heath, G. *Land-Use Requirements for Solar Power Plants in the United States*; National Renewable Energy Laboratory (NREL): Golden, CO, USA, 2013. [CrossRef]
25. Skoplaki, E.; Palyvos, J.A. On the temperature dependence of photovoltaic module electrical performance: A review of efficiency/power correlations. *Sol. Energy* **2009**, *83*, 614–624. [CrossRef]
26. Söder, L.; Ackermann, T. Wind Power in Power Systems: An Introduction. In *Wind Power in Power Systems*, 1st ed.; Ackermann, T., Ed.; Wiley: Chichester, UK, 2005; pp. 25–52.
27. Maanmittauslaitos—Karttapaikka. Available online: https://asiointi.maanmittauslaitos.fi/karttapaikka/ (accessed on 11 April 2023).

28. Hadi, F.A. Diagnosis of the Best Method for Wind Speed Extrapolation. *Int. J. Adv. Res. Electr. Electron. Instrum. Eng.* **2015**, *4*, 8176–8183. [CrossRef]
29. Sumair, M.; Aized, T.; Gardezi, S. Extrapolation of wind data using generalized versus site-specific wind power law for wind power production prospective at Shahbandar—A coastal site in Pakistan. *Energy Explor. Exploit.* **2021**, *39*, 2240–2256. [CrossRef]
30. Carrillo, C.; Obando Montaño, A.F.; Cidrás, J.; Díaz-Dorado, E. Review of power curve modelling for wind turbines. *Renew. Sustain. Energy Rev.* **2013**, *21*, 572–581. [CrossRef]
31. Rahman, S.; Akther, S.; Hoque, H.E. Comparison of Different Pitch Controller in Wind Farm for Integrated Power System. *Am. J. Eng. Res. (AJER)* **2018**, *7*, 288–299. [CrossRef]
32. Okedu, K.E. Effect of ECS low-pass filter timing on grid frequency dynamics of a power network considering wind energy penetration. *IET Renew. Power Gener.* **2017**, *11*, 1194–1199. [CrossRef]
33. Chae, S.H.; Kang, C.U.; Kim, E.-H. Field Test of Wind Power Output Fluctuation Control Using an Energy Storage System on Jeju Island. *Energies* **2020**, *13*, 5760. [CrossRef]
34. Thiringer, T.; Linders, J. Control by Variable Rotor Speed of a Fixed-Pitch Wind Turbine Operating in a Wide Speed Range. *IEEE Trans. Energy Convers.* **1993**, *8*, 520–526. [CrossRef]
35. RyseEnergy. Available online: https://www.ryse.energy/10kw-wind-turbines/ (accessed on 6 April 2023).
36. Wind-Turbine-Models.com. Available online: https://en.wind-turbine-models.com/turbines/1829-aeolia-windtech-d2cf-200 (accessed on 6 April 2023).
37. Wind-Turbine-Models.com. Available online: https://en.wind-turbine-models.com/turbines/114-enercon-e-58-10.58 (accessed on 6 April 2023).
38. Wind-Watch. Available online: https://docs.wind-watch.org/Enercon.pdf (accessed on 6 April 2023).
39. Lappalainen, K.; Kleissl, J. Analysis of the cloud enhancement phenomenon and its effects on photovoltaic generators based on cloud speed sensor measurements. *J. Renew. Sustain. Energy* **2020**, *12*, 043502. [CrossRef]
40. Tang, C.; Pathmanathan, M.; Soong, W.L.; Ertugrul, N. Effects of Inertia on Dynamic Performance of Wind Turbines. In Proceedings of the 2008 Australasian Universities Power Engineering Conference, Sydney, Australia, 14–17 December 2008.